Carrier-Envelope-Phase Characterization for an Isolated Attosecond Pulse by Angular Streaking

Pei-Lun He,[1] Camilo Ruiz,[2] and Feng He[1,*]

[1]*Key Laboratory for Laser Plasmas (Ministry of Education) and Department of Physics and Astronomy, Collaborative Innovation Center of IFSA (CICIFSA), Shanghai Jiao Tong University, Shanghai 200240, China*

[2]*Departamento de Física de Partículas, Universidad de Santiago de Compostela, E-15782 Santiago de Compostela, Spain*

(Received 26 August 2015; published 18 May 2016)

The carrier envelope phase (CEP) is a crucial parameter for a few-cycle laser pulse since it substantially determines the laser waveform. Stepping forward from infrared to extreme ultraviolet (EUV) pulses, we propose a strategy to directly characterize the CEP of an isolated attosecond pulse (IAP) by numerically simulating the tunneling ionization of a hydrogen atom in a combined IAP and phase-stabilized circularly polarized IR laser pulse. The fine modulations of the combined laser fields, due to the variation of the CEP of the IAP, are exponentially enlarged onto the distinct time-dependent tunneling ionization rate. Electrons released at different time with distinct tunneling ionization rates are angularly streaked to different directions. By measuring the resulting photoelectron momentum distribution, the CEP of the IAP can be retrieved. The characterization of the CEP of an IAP will open the possibility of capturing sub-EUV-cycle dynamics.

DOI: 10.1103/PhysRevLett.116.203601

The CEP of a few-cycle laser pulse determines its electric field, which in turn, governs many strong field processes observed in ultrafast physics [1]. The availability of few-cycle CEP-stabilized IR laser pulses [2,3] opens the possibility of capturing the subcycle dynamics in atoms and molecules. Over the last few decades, a series of interesting phenomena have been explored using few-cycle CEP-locked IR pulses. For example, Lindner *et al.* controlled the electron ejection from an atom at one of two possible instants, producing a Young's double-slit type interference in the photoelectron energy spectra [4]. Kling *et al.* steered the electron movement in a subcycle time scale and controlled the path of molecular breakup [5]. Baltuška *et al.* generated supercontinuum high harmonics [6], which could be synthesized into an IAP [7]. The IAP provides accesses to unprecedented high time resolution and has boosted ultrafast sciences into attosecond time scales [1]. By combining an IAP and CEP-locked IR pulse, people have successfully observed many ultrafast processes with attosecond resolutions, such as Auger decay [8], direct measurement of a few-cycle light wave [9], time delay in photoionization [10], tunneling processes [11], charge directional steering [12–14], control of absorption line shapes [15], and many others.

The CEP of a few-cycle strong IR pulse has been characterized with several methods [16–20]. All these methods fundamentally depend on the tunneling ionization of atoms in strong laser fields. When the CEP of the IR laser pulse is varied, the symmetry of the laser waveform is modified. The slight and subcycle modification of the laser waveform is magnified into the photoelectron since the tunneling ionization is highly nonlinear. By diagnosing the asymmetric photoelectron energy spectra, one may extract the CEP information [17] in a single shot. The tunneled electron may rescatter with its parent ion and emit high harmonics, where the CEP information is also imprinted [21].

The successful characterization of the CEP of a few-cycle strong IR pulse motivates us to undertake the ambitious task of characterizing the CEP of an IAP. Compared to a few-cycle CEP-stabilized IR field, a few-cycle CEP-stabilized IAP will make it possible to access dynamics in the sub-EUV period. Few-cycle IAPs have already been produced in many labs with different strategies [7,22–25]. Unfortunately, the concepts which work well for strong IR pulses cannot be directly applied to characterize the CEP of an IAP because the IAP in most labs is currently far too weak to sustain highly nonlinear processes. The characterization of attosecond pulses is normally performed using the reconstruction of attosecond beating by interference of two-photon transitions (RABBIT) [26] or frequency-resolved optical gating for complete reconstruction of attosecond burst (FROGCRAB) [27] methods. Both methods are accurate but are limited to characterize the temporal envelope and the spectral phase of a pulse. The characterization of the CEP of an IAP is still a big challenge.

In this Letter, we propose to use the angular streaking technique to characterize the CEP of an IAP. Note that angular streaking cameras have been used to unveil several interesting phenomena [28–31]. In our strategy, the prototypical hydrogen atom is tunneling ionized by the

overlapped IAP-IR field. The variation of the CEP of the weak IAP only slightly modifies the overlapped laser waveform, but substantially changes the instantaneous tunneling ionization rate. Thus, the electrons released with IAP-CEP-dependent ionization rates are angularly streaked to different directions, and the CEP of the IAP is mapped onto the photoelectron angular distribution. Importantly, the IR intensity must be strong enough to guarantee the highly nonlinear tunneling ionization, and be circularly or elliptically polarized to resolve the photoelectron distribution into the laser polarization plane.

We sketched the principle of our method in Fig. 1. The combined IAP and IR fields are presented in 1(a), where the thick red part highlights the overlapped electric fields. Panel 1(b) shows the scaled photoelectron probability angular distribution estimated by the ADK theory [32]. Both circularly polarized pulses are expressed as

$$\mathbf{E}_i(t) = E_{0,i}[\cos(\omega_i t+\theta_i)\hat{x} - \sin(\omega_i t+\theta_i)\hat{y}]\cos^2\left(\pi\frac{t}{\tau_i}\right), \quad -\tau_i/2 < t < \tau_i/2, \tag{1}$$

where i represents the IAP or IR pulse, τ_i is the pulse duration, θ_i is the CEP. The electric amplitude is defined as $E_{0,i} = (I_i/3.51\times10^{16})^{1/2}$ a.u., with I_i being the intensity. In later simulations, both the IAP and IR pulse have four cycles. The IR wavelength is 800 nm. The electric fields $\mathbf{E}_i(t)$ rotate clockwise in the x-y plane. At the moment that $\mathbf{E}_{\mathrm{IAP}}(t)$ and $\mathbf{E}_{\mathrm{IR}}(t)$ are parallel, the addition of those two produces a local maximum field, which will result in a maximum tunneling ionization rate, as marked by the solid square. Conversely, at the moment that $\mathbf{E}_{\mathrm{IAP}}(t)$ and $\mathbf{E}_{\mathrm{IR}}(t)$ are antiparallel, the subtraction leads to a local minimum tunneling ionization rate, as marked by the solid circle. Note that the tunneling ionization rate exponentially depends on the superimposed electric field, thus the local maximum and minimum rates are distinct even if the IAP is very weak. Electrons released at different time will be streaked by the later electric field, acquiring the momentum equating to the laser vector potential at the tunneling time if the Coulomb potential is not considered [33]. If the CEP of the IAP is shifted, the positions of the local minima and maxima of the combined electric field will also shift in the polarization plane, which is imprinted in the photoelectron angular distribution. In principle, this method works for an IAP with arbitrary wavelength and arbitrary polarization. To extract the CEP of the IAP, the photoelectron angular distribution is measured and then compared with the results from the standard time dependent Schrödinger equation (TDSE) simulation.

When the hydrogen atom is exposed to the combined IAP and IR pulse, the strong field approximation (SFA) gives the following photoionization amplitude (atomic units are used throughout unless stated otherwise)

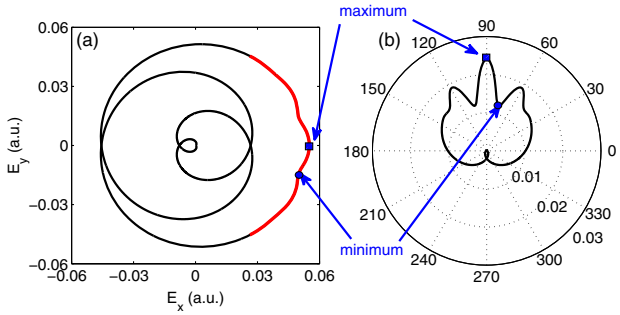

FIG. 1. (a) The superimposed IAP and IR electric field. The red thick curve indicates the overlapped part. (b) The angular resolved ionization rate estimated by the ADK theory without including the Coulomb action on the tunneled electron. The solid squares and circles indicate the maximum and minimum ionization rates induced by the addition or subtraction of two fields, respectively. The central wavelength of the IAP is 67 nm. $I_{\mathrm{IAP}} = 2\times10^{11}$ W/cm^2 and $I_{\mathrm{IR}} = 2\times10^{14}$ W/cm^2, $\theta_{\mathrm{IAP}} = \theta_{\mathrm{IR}} = 0$.

$$M(\mathbf{p}) = -i\int dt e^{i\phi(t)}\mathbf{d}[\mathbf{p}+\mathbf{A}_{\mathrm{IAP}}(t)+\mathbf{A}_{\mathrm{IR}}(t)] \cdot [\mathbf{E}_{\mathrm{IAP}}(t)+\mathbf{E}_{\mathrm{IR}}(t)], \tag{2}$$

where the phase $\phi(t)$ is written as

$$\phi(t) = \mathrm{I}_p(t-t_0) + \int_{t_0}^{t} dt' \frac{[\mathbf{p}+\mathbf{A}_{\mathrm{IAP}}(t')+\mathbf{A}_{\mathrm{IR}}(t')]^2}{2}, \tag{3}$$

with $\mathrm{I}_p = 0.5$ a.u. being the ionization potential, $\mathbf{A}_{\mathrm{IAP}}$ and $\mathbf{A}_{\mathrm{IR}}$ being the IAP and IR vector potentials, and t_0 being the starting time of the laser pulse. In Eq. (2) $\mathbf{d}(\mathbf{p}) \propto [\mathbf{p}/(\mathbf{p}^2+2I_p)^3]$ is the transition dipole. The modulus square of the transition amplitude can be written explicitly

$$|M(\mathbf{p})|^2 = \left|\int dt e^{i\phi(t)}\mathbf{d}\cdot\mathbf{E}_{\mathrm{IR}}(t)\right|^2 + \left|\int dt e^{i\phi(t)}\mathbf{d}\cdot\mathbf{E}_{\mathrm{IAP}}(t)\right|^2 + 2\mathrm{Re}\left[\left(\int dt e^{i\phi(t)}\mathbf{d}\cdot\mathbf{E}_{\mathrm{IAP}}(t)\right)\left(\int dt e^{i\phi(t)}\mathbf{d}\cdot\mathbf{E}_{\mathrm{IR}}(t)\right)^*\right]. \tag{4}$$

For convenience, three terms on the right-hand side of Eq. (4) are named as T_1, T_2, and T_3. T_2 describes the conventional angular streaking [34]. The IR intensity here must be strong enough to tunneling ionize the hydrogen atom, thus T_1 and T_3 must be taken into account. This is fundamentally different from the well-established linear or circular streaking techniques [9,34]. The T_3 term is the main one responsible for the distinct ionization rate which is mapped onto the photoelectron angular distribution and depends strongly on the CEP of the IAP.

Figure 2 plots T_1, T_2, T_3, and $|M(\mathbf{p})|^2$ in panels from left to right when the IAP wavelengths are 67 nm (upper row) and 100 nm (lower row), respectively. For reference, Figs. 2(e) and 2(j) show the photoelectron momentum

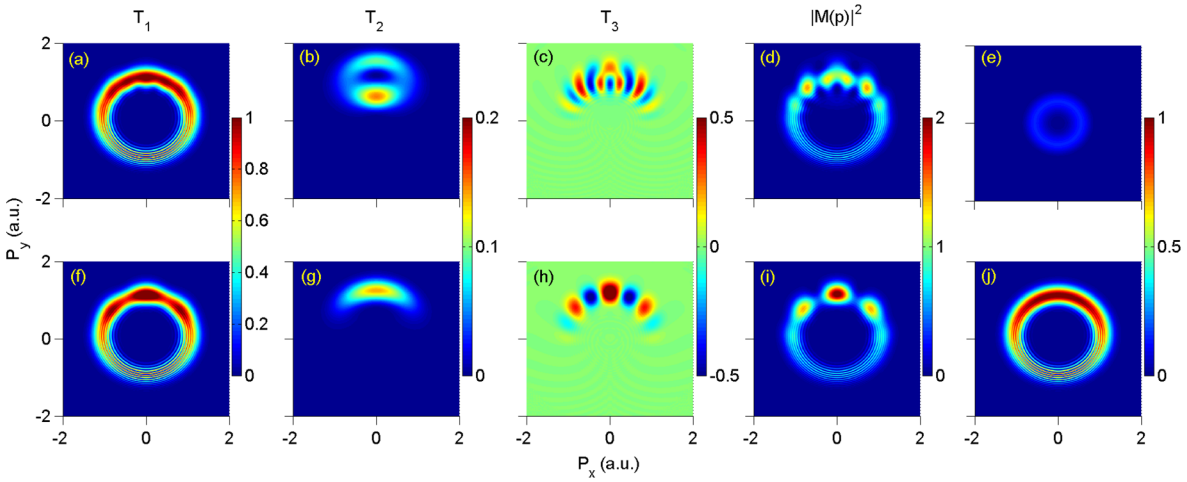

FIG. 2. The photoelectron momentum distribution in the laser polarization plane (i.e., $p_z = 0$) contributed by T_1 (a),(f), T_2 (b),(g), T_3 (c),(h), and the addition of these three terms (d),(i). The upper and lower rows are for the IAP wavelengths 67 and 100 nm, respectively. (e) and (j) the photoelectron momentum distribution when only the EUV (67 nm) and only the IR field are used, respectively. $I_{\mathrm{IAP}} = 2 \times 10^{11}$ W/cm^2, $I_{\mathrm{IR}} = 2 \times 10^{14}$ W/cm^2, $\theta_{\mathrm{IAP}} = \theta_{\mathrm{IR}} = 0$.

distributions when only the EUV (67 nm) and only the IR pulse are used, respectively. In 2(a), 2(d), 2(f), and 2(i), the photoelectron momentum distributions present circles having the radius of the IR vector potential. Compared to Fig. 2(j), the small angular fluctuations in Fig. 2(a), which are more clearly visible in Fig. 2(f), are contributed by the IAP term in $\phi(t)$. In the absence of strong IR fields, the circularly polarized IAP generates the photoelectron with rotationally symmetric momentum distribution having radius $\sqrt{2(\omega_{\mathrm{IAP}} - I_p)}$ when the single IAP photon energy is larger than the ionization potential, as shown in Fig. 2(e). The two lobes located around at $p_y = 0.8$ and 1.4 a.u. in Fig. 2(b) are evolved from the photoelectron having opposite momenta just before streaking. However, the two lobes shrink together if the EUV photon energy is less than the ionization potential and the IR field is present, as shown in Fig. 2(g). Figures 2(c) and 2(h) show sawtoothlike structures, which depend on the CEP of the IAP sensitively. Note that 2(c) and 2(h) have positive and negative parts, thus T_3 actually increases or suppresses the instantaneous photoionization rate. The angular modulation of the photoelectron momentum is still clear after adding T_1, T_2, and T_3, which means that it is possible to retrieve the CEP of the IAP by inspecting the photoelectron momentum angular distribution in future experiments. According to Eq. (4), T_3 depends on θ_{IR} and θ_{IAP}, which is a precise analog to the f-$2f$ method [2,3], which measures the interference beat frequency between the high frequency and the frequency-doubled low frequency spectral components of an octave spanning spectrum. The IR-intensity dependence of the photoelectron momentum distribution can be read in the Supplemental Material [35].

The SFA is straightforward to explain the principle of our technique, however, in order to extract the accurate CEP of the IAP by means of comparing experimental measurements and theoretical calculations, one needs to simulate the three-dimensional TDSE numerically

$$i\frac{\partial\Psi(x,y,z;t)}{\partial t} = \left[\frac{[p_x + A_x(t)]^2}{2} + \frac{[p_y + A_y(t)]^2}{2} + \frac{p_z^2}{2} - \frac{1}{\sqrt{x^2+y^2+z^2}}\right]\Psi(x,y,z;t), \quad (5)$$

where p_i $(i = x, y, z)$ is the momentum operator. We used the split operator method to propagate the wave function. The initial state was obtained by imaginary time propagation. The sample grids are $2500 \times 2500 \times 200$ in the three-dimensional x-y-z simulation box, and spatial steps are $\Delta x = \Delta y = \Delta z = 0.3$ a.u. The time step is $\Delta t = 0.1$ a.u. The simulation box is big enough to prevent the wave packet from hitting the boundaries during the whole calculation. We propagated the wave function enough time after the laser field was finished in order to obtain converged physical observations. $W(p_x, p_y, \mathrm{CEP})$, the photoelectron momentum distribution in the laser polarization plane, is obtained by projecting the ionized wave packet (in the area $\sqrt{x^2+y^2+z^2} > 50$ a.u.) into plane waves at the end of the calculation and then integrating over p_z. Further, after integrating the photoelectron momentum radially, we obtained the CEP-dependent photoelectron angular distribution $A(\alpha, \mathrm{CEP})$, where α is the polar angle and $\alpha = \mathrm{Arg}(p_x + ip_y)$.

Figure 3(a) shows the calculated $A(\alpha, \mathrm{CEP})$ when the circularly polarized IAP has the central wavelength 100 nm and the intensity 2×10^{11} W/cm^2, and the IR intensity is 2×10^{14} W/cm^2. Similar results are shown in Fig. 3(b), but for a helium target with the IR intensity 6×10^{14} W/cm^2 and EUV intensity 10^{10} W/cm^2. A modeled Coulomb potential [36] was used for helium calculations. The observed structures clearly demonstrate that the CEP of

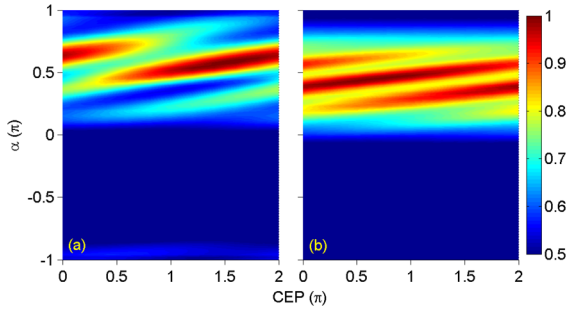

FIG. 3. The photoelectron probability distribution as a function of the polar angle α and the CEP of the IAP calculated for (a) hydrogen and (b) helium. In (a), $I_{\mathrm{IAP}} = 2 \times 10^{11}$ W/cm^2, $I_{\mathrm{IR}} = 2 \times 10^{14}$ W/cm^2. In (b), $I_{\mathrm{IAP}} = 10^{10}$ W/cm^2, $I_{\mathrm{IR}} = 6 \times 10^{14}$ W/cm^2. $\theta_{\mathrm{IR}} = 0$. Both panels have been normalized by their own maxima.

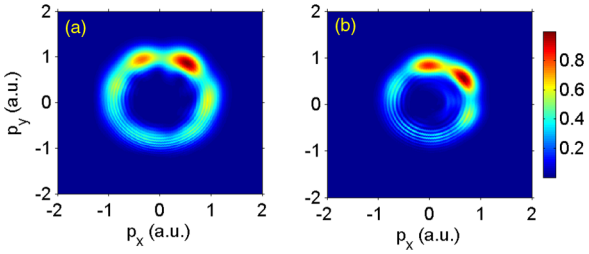

FIG. 4. (a) The photoelectron momentum distribution after averaging the focal volume intensity. The IR peak intensity is 2.5×10^{14} W/cm^2, and the IAP intensity is 2×10^{11} W/cm^2. $\theta_{\mathrm{IAP}} = 0$, $\theta_{\mathrm{IR}} = 0.5\pi$. (b) The photoelectron momentum distribution after averaging the CEP jitter of the IR pulse, which randomly distributes within $[0.5\pi, 0.65\pi]$. The IR intensity is fixed at 10^{14} W/cm^2, $\theta_{\mathrm{IAP}} = 0$. Both panels have been normalized by their own maxima.

the IAP is mapped into the photoelectron angular distribution. Theoretically, each stripe spans an angle $2\pi/(\omega_{\mathrm{IAP}}/\omega_{\mathrm{IR}} - 1)$, thus a smaller frequency ratio $\omega_{\mathrm{IAP}}/\omega_{\mathrm{IR}}$ will be in favor of having a better signal-to-noise ratio in experiment.

To try out our strategy in experiment, it is important to carefully consider several sources of noise which might blur the fringes, such as the focal volume intensity average, the average of the CEP jitter of the IR pulse. Neither the intensity averaging in the focus nor the difficulty to precisely measure the value of the IR peak intensity affects the measurement of the CEP in our proposal. We calculated the photoelectron momentum distributions when the IR pulse has a peak intensity 2.5×10^{14} W/cm^2 and a Gaussian spatial distribution. We showed the photoelectron momentum distribution in Fig. 4(a) after counting on the focal volume intensity average effect [37]. One may clearly see that the angular nodes are not smeared out after summing up photoelectron distributions induced by different laser intensities.

Our strategy is fundamentally different from other proposals [14,38,39]. For example, Sansone *et al.* [14] proposed to characterize the CEP of the IAP by reading the interference pattern induced by both the EUV and IR in the ionization. This idea was numerically implemented by Peng *et al.* [38] using the EUV intensity around 10^{15} W/cm^2. Liu *et al.* [39] suggested extracting the CEP of the IAP by looking into the interference of the EUV-triggered ionization and the IR-induced rescattering ionization events, which requires very stable IR CEP and intensities. In our strategy, the photoelectron angular distribution is due to the variation of the superimposed instantaneous IAP and IR fields. Our strategy is robust because it works for very weak IAP and it is not necessary for the IR intensity to be very stable. Actually, this weak dependence on the intensity of the photoelectron momentum distribution is one of the biggest advantages of our strategy, as it is notoriously difficult to precise determine the IR intensity, though the most accurate measurement for the laser intensity has achieved 1% [40].

Similar to other proposals [14,38,39], the stability of the CEP of the IR pulses is a very critical parameter. In our strategy, the CEP jitter of the IAP, $\delta\theta_{\mathrm{IAP}}$, connects to the CEP jitter of the IR pulse, $\delta\theta_{\mathrm{IR}}$, through $\delta\theta_{\mathrm{IAP}} = (\omega_{\mathrm{IAP}}/\omega_{\mathrm{IR}})\delta\theta_{\mathrm{IR}}$. When the EUV is 100 nm, the angle between two neighboring maxima for the photoelectron angular distribution as shown in Fig. 3(a) is $2\pi/7$. To resolve the angular nodes, $\delta\theta_{\mathrm{IR}}$ must be smaller than $\pi/7$. In Fig. 4(b) we show the photoelectron momentum angular distribution after averaging the CEP of the IR varying within $[0.5\pi, 0.65\pi]$. The angular nodes are still clearly seen. We numerically tested that when the CEP jitter of the IR pulse is about 0.2π, the angular nodes will be smeared out and this angular streaking strategy will be destroyed. To achieve the CEP of the IAP with the accuracy $\delta\theta_{\mathrm{IAP}} < 0.1\pi$, $\delta\theta_{\mathrm{IR}}$ must be smaller than 40 mrad. Fortunately, the CEP jitters of IR pulses in experiment can be determined with smaller and smaller uncertainties, from 200 [41] to 60 [42,43], and even 20 mrad [44] with developing techniques. Hence, we claim that the current laser technology in some advanced labs is ready to confirm our proposal. More simulation results show the chirp and time profile of the IAP nearly do not influence the photoelectron momentum distribution, allowing our proposal to work properly.

To summarize, due to the highly nonlinear characteristic of tunneling ionization, the tiny variations in the electric field produced by the changes in the CEP of a weak IAP are exponentially enlarged onto the ionization rate, resulting in the CEP-dependent photoelectron momentum distribution angularly streaked in the laser polarization plane. Based on this principle, one may retrieve the absolute CEP of an IAP from the photoelectron angular distribution. Our strategy is robust because it works regardless of the IAP wavelength, intensity, polarization, and chirp. The CEP characterization of an IAP will push ultrafast physics into much shorter time scales and unveil a lot of new exciting physics, for example,

exploring the sensitive ionization by EUV pulses [45], tracing the relativistic movement of electrons in highly charged ions.

This work was supported by the NSF of China (Grants No. 11322438, No. 11574205, No. 11327902). Simulations were performed on the π supercomputer at Shanghai Jiao Tong University.

*fhe@sjtu.edu.cn

[1] F. Krausz and M. Ivanov, Rev. Mod. Phys. **81**, 163 (2009).
[2] A. Apolonski, A. Poppe, G. Tempea, C. Spielmann, T. Udem, R. Holzwarth, T. W. Hänsch, and F. Krausz, Phys. Rev. Lett. **85**, 740 (2000).
[3] D. J. Jones, S. A. Diddams, J. K. Ranka *et al.*, Science **288**, 635 (2000).
[4] F. Lindner, M. G. Schätzel, H. Walther, A. Baltuska, E. Goulielmakis, F. Krausz, D. B. Milosevic, D. Bauer, W. Becker, and G. G. Paulus, Phys. Rev. Lett. **95**, 040401 (2005).
[5] M. F. Kling, Ch. Siedschlag, A. J. Verhoef, J. I. Khan, M. Schultze, Th. Uphues, Y. Ni, M. Uiberacker, M. Drescher, F. Krausz, and M. J. J. Vrakking, Science **312**, 246 (2006).
[6] A. Baltuška, Th. Udem, M. Uiberacker, M. Hentschel, E. Goulielmakis, Ch. Gohle, R. Holzwarth, V. S. Yakovlev, A. Scrinzi, T. W. Hänsch, and F. Krausz, Nature (London) **421**, 611 (2003).
[7] M. Hentschel, R. Kienberger, Ch. Spielmann, G. A. Reider, N. Milosevic, T. Brabec, P. Corkum, U. Heinzmann, M. Drescher, and F. Krausz, Nature (London) **414**, 509 (2001).
[8] M. Drescher, M. Hentschel, R. Kienberger, M. Uiberacker, V. Yakovlev, A. Scrinzi, Th. Westerwalbesloh, U. Kleineberg, U. Heinzmann, and F. Krausz, Nature (London) **419**, 803 (2002).
[9] E. Goulielmakis, M. Uiberacker, R. Kienberger1, A. Baltuska, V. Yakovlev, A. Scrinzi, Th. Westerwalbesloh, U. Kleineberg, U. Heinzmann, M. Drescher, and F. Krausz, Science **305**, 1267 (2004).
[10] M. Schultze, M. Fieß, N. Karpowicz, J. Gagnon, M. Korbman, M. Hofstetter, S. Neppl, A. L. Cavalieri, Y. Komninos, Th. Mercouris *et al.*, Science **328**, 1658 (2010).
[11] M. Uiberacker, Th. Uphues, M. Schultze, A. J. Verhoef, V. Yakovlev, M. F. Kling, J. Rauschenberger, N. M. Kabachnik, H. Schröder, M. Lezius *et al.* Nature (London) **446**, 627 (2007).
[12] F. He, C. Ruiz, and A. Becker, Phys. Rev. Lett.**99**, 083002 (2007).
[13] F. He, A. Becker, and U. Thumm, Phys. Rev. Lett. **101**, 213002 (2008).
[14] G. Sansone, F. Kelkensberg, J. F. Pérez-Torres, F. Morales, M. F. Kling, W. Siu, O. Ghafur, P. Johnsson, M. Swoboda, E. Benedetti *et al.* Nature (London) **465**, 763 (2010).
[15] C. Ott, A. Kaldun, P. Raith, K. Meyer, M. Laux, J. Evers, C. H. Keitel, C. H. Greene, and T. Pfeifer, Science **340**, 716 (2013).
[16] G. G. Paulus, F. Lindner, H. Walther, A. Baltuska, E. Goulielmakis, M. Lezius, and F. Krausz, Phys. Rev. Lett. **91**, 253004 (2003).
[17] T. Wittmann, B. Horvath, W. Helml, M. G. Schätzel, X. Gu, A. L. Cavalieri, G. G. Paulus, and R. Kienberger, Nat. Phys.**5**, 357 (2009).
[18] S. Micheau, Zh. Chen, T. Morishita, A.-T. Le, and C. D. Lin, J. Phys. B **42**, 065402 (2009).
[19] T Rathje, N. G Johnson, M. Möller, F. Süßmann, D. Adolph, M. Kübel, R. Kienberger, M. F. Kling, G. G. Paulus, and A. M. Sayler, J. Phys. B **45**, 074003 (2012).
[20] V. V. Strelkov, E. Mevel, and E. Constant, Opt. Express **22**, 6239 (2014).
[21] P. Ye, X. He, H. Teng, M. Zhan, S. Zhong, W. Zhang, L. Wang, and Zhiyi Wei, Phys. Rev. Lett. **113**, 073601 (2014).
[22] G. Sansone, E. Benedetti, F. Calegari, C. Vozzi, L. Avaldi, R. Flammini, L. Poletto, P. Villoresi, C. Altucci, R. Velotta, S. Stagira, S. De Silvestri, and M. Nisoli, Science **314**, 443 (2006).
[23] H. Mashiko, S. Gilbertson, C. Li, S. D. Khan, M. M. Shakya, E. Moon, and Z. Chang, Phys. Rev. Lett. **100**, 103906 (2008).
[24] J. A. Wheeler, A. Borot, S. Monchocé, Henri Vincenti, A. Ricci, A. Malvache, R. Lopez-Martens, and F. Quéré, Nat. Photonics **6**, 829 (2012).
[25] M. J. Abel, T. Pfeifer, P. M. Nagel, W. Boutu, M. J. Bell, C. P. Steiner, D. M. Neumark, and S. R. Leone, Chem. Phys. **366**, 9 (2009).
[26] P. M. Paul, E. S. Toma, P. Breger, G. Mullot, F. Augá, Ph. Balcou, H. G. Muller, and P. Agostini, Science **292**, 1689 (2001).
[27] Y. Mairesse and F. Quéré, Phys. Rev. A **71**, 011401(R) (2005).
[28] A. N. Pfeiffer, C. Cirelli, M. Smolarski, R. Dörner, and U. Keller, Nat. Phys. **7**, 428 (2011).
[29] P. Eckle, A. N. Pfeiffer, C. Cirelli, A. Staudte, R. Dörner, H. G. Muller, M. Büttiker, and U. Keller, Science **322**, 1525 (2008).
[30] M. Ivanov and O. Smirnova, Phys. Rev. Lett. **107**, 213605 (2011).
[31] J. Wu, M. Magrakvelidze, L. P. H. Schmidt, M. Kunitski, T. Pfeifer, M. Schöffler, M. Pitzer, M. Richter, S. Voss, H. Sann *et al.*, Nat. Commun. **4**, 2177 (2013).
[32] M. V. Ammosov, N. B. Delone, and V. P. Krainov, Zh. Eksp. Teor. Fiz. **91**, 2008 (1986) [Sov. Phys. JETP **64**, 1191 (1986)].
[33] P. L. He, N. Takemoto, and F. He, Phys. Rev. A **91**, 063413 (2015).
[34] J. Itatani, F. Quéré, G. L. Yudin, M. Yu. Ivanov, F. Krausz, and P. B. Corkum, Phys. Rev. Lett. **88**, 173903 (2002).
[35] See Supplemental Material at http://link.aps.org/supplemental/10.1103/PhysRevLett.116.203601 for movies. The first movie shows the photoelectron momentum distribution when the IR intensity increases. The second movie shows the photoelectron angular distribution when the CEP of the IAP is scanned.
[36] X. M. Tong and C. D. Lin, J. Phys. B **38**, 2593 (2005).
[37] A. S. Alnaser, X. M. Tong, T. Osipov, S. Voss, C. M. Maharjan, B. Shan, Z. Chang, and C. L. Cocke, Phys. Rev. A **70**, 023413 (2004).
[38] L. Y. Peng, E. A Pronin, and A. F. Starace, New J. Phys. **10**, 025030 (2008).

[39] C. D. Liu, M. Reduzzi, A. Trabattoni, A. Sunilkumar, A. Dubrouil, F. Calegari, M. Nisoli, and G. Sansone, Phys. Rev. Lett. **111**, 123901 (2013).

[40] M. G. Pullen, W. C. Wallace, D. E. Laban, A. J. Palmer, G. F. Hanne, A. N. Grum-Grzhimailo, K. Bartschat, I. Ivanov, A. Kheifets, D. Wells *et al.*, Phys. Rev. A **87**, 053411 (2013).

[41] A. M. Sayler, M. Arbeiter, S. Fasold, D. Adolph, M. Möller, D. Hoff, T. Rathje, B. Fetić, D. B. Milošević, T. Fennel, and G. G. Paulus, Opt. Lett. **40**, 3137 (2015).

[42] M. Zhan, P. Ye, H. Teng, X. He, W. Zhang, S. Zhong, L. Wang, C. Yun, and Z. Wei, Chin. Phys. Lett. **30**, 093201 (2013).

[43] W. Zhang, H. Teng, C. Yun, P. Ye, M. Zhan, S. Zhong, X. He, L. Wang, and Z. Wei, Chin. Phys. Lett. **31**, 084204 (2014).

[44] B. Borchers, S. Koke, A. Husakou, J. Herrmann, and G. Steinmeyer, Opt. Lett. **36**, 4146 (2011).

[45] I. A. Ivanov, A. S. Kheifets, K. Bartschat, J. Emmons, S. M. Buczek, E. V. Gryzlova, and A. N. Grum-Grzhimailo, Phys. Rev. A **90**, 043401 (2014).